Supplementary materials for

Experimental determination of Si, Mg, and Ca isotope fractionation during enstatite melt evaporation

Wenhua Lu[1,2,3†], Richard Weber[4], Zhaofeng Zhang[5], Yuan Li[1,2]

[1]State Key Laboratory of Isotope Geochemistry, Guangzhou Institute of Geochemistry, Chinese Academy of Sciences, Guangzhou 510640, China
[2]CAS Center for Excellence in Deep Earth Science, Guangzhou, 510640, China
[3]College of Earth and Planetary Sciences, University of Chinese Academy of Sciences, Beijing 100049, China
[4]Materials Development, Inc., 3090 Daniels Court, Arlington Heights, IL 60004, USA
[5]International Center for Planetary Science, College of Geosciences, Chengdu University of Technology, Chengdu 610059, China

[†]Corresponding author: Wenhua Lu (wenhualu@gig.ac.cn).

Contents of this file:

Text S1. Estimating the effect of temperature fluctuation on the run duration at the target temperature

Temperature fluctuation is hard to avoid in levitation experiments (e.g., Badro et al., 2021), because shaking is inevitable for the levitated sample, which constantly loses its mass in the flowing gas. The temperature fluctuation was ~50 K on average for most of our experiments, but temperature fluctuation over 100 K occasionally occurred in a few experiments (Figure S1). Taking the laser running duration as the heating duration at the target temperature would be incorrect for the experiments with considerable temperature fluctuation. We therefore corrected the heating duration by using the procedure as described in Ni et al. (2021).

Chemical reaction on the evaporating surface for an oxide of element i could be written as:

$$iO_{(x+q)/2}\ (melt) = iO_{x/2}\ (gas) + q/4\ O_2\ (gas) \quad (S1)$$

where x is the charge of i in the gas and q is the number of electrons transferred. Assuming that the fugacity coefficient of the gaseous i-bearing species is 1, the equilibrium constant K_i of this reaction could be written as:

$$K_i = \frac{P_{i,sat}\,(fO_2)^{q/4}}{\gamma_i X_i} \quad (S2)$$

where $P_{i,sat}$ is the equilibrium partial pressure of i; fO_2 is the oxygen fugacity; γ_i and X_i are the activity coefficient and molar fraction of the $iO_{(x+q)/2}$ in the melt, respectively. The X_i in Eq. (S2) could be converted to the number of mole of the $iO_{(x+q)/2}$ in the melt (n_i) with a total number of mole, n_{total}, via:

$$X_i = \frac{n_i}{n_{total}} = \frac{n_i}{\rho_{melt} V / M_{melt}} \quad (S3)$$

where ρ_{melt}, V, and M_{melt} are the density, volume, and the molar mass of the melt, respectively. According to the Hertz-Knudsen equation, the net evaporation flux of i (dn_i/dt in mol/s) evaporated from the melt sphere is (Dauphas et al., 2015; Richter et al., 2007; Sossi et al., 2019):

$$\frac{dn_i}{dt} = -4\pi r^2 \frac{\varepsilon_i (P_{i,sat} - P_i)}{\sqrt{2\pi M_i RT}} \quad (S4)$$

where ε_i is the evaporation coefficient of i; P_i and M_i are the partial pressure and molar mass of i-bearing gaseous species at the surface, respectively; R is the gas constant; T is the temperature in K; r is the radio of the melt sphere. Define the saturation degree S as:

$$S = P_i / P_{i,sat} \quad (S5).$$

The combination of Eqs. (S2) to (S5) would yield:

$$\frac{dn_i}{n_i} = -\frac{3\varepsilon_i K_i \gamma_i M_{melt}\,(1-S)}{r\rho_{melt}\,(fO_2)^{q/4}\sqrt{2\pi M_i RT}}\,dt \quad (S6).$$

In Eq. (S6), K_i can be thermodynamically expressed as:

$$K_i = \exp\left(\frac{\Delta_f G}{-RT}\right) \quad (S7)$$

where $\Delta_f G$ is the Gibbs free energy change of the surface reaction (Eq. (S1)). Assuming that K_i is the only temperature-dependent factor in Eq. (S6), we defined a new parameter Φ_i:

$$\Phi_i = -\frac{\varepsilon_i \gamma_i M_{melt}\,(1-S)}{r\rho_{melt}\,(fO_2)^{q/4}\sqrt{2\pi M_i R}} \quad (S8)$$

which represents the rest temperature-independent parameters in Eq. (S6). Then, a simplified form of Eq. (S6) could be written as:

$$\frac{dn_i}{n_i} = -\frac{\Phi_i}{\sqrt{T}}\exp\left(\frac{\Delta_f G}{-RT}\right)dt \quad (S9).$$

For an ideal experiment in which the silicate melt evaporates at a target temperature T_0 without any temperature fluctuation, the value of $n_{i,tc}$ relative to its initial $n_{i,0}$ in the melt after a duration t_c could be obtained through integrating both sides of Eq. (S9):

$$\ln\frac{n_{i,t_c}}{n_{i,0}} = -\frac{\Phi_i}{\sqrt{T_0}}\exp\left(\frac{\Delta_f G}{-RT_0}\right)t_c \quad (S10).$$

The integration of the right side of Eq. (S9) could be also expressed in discrete form applying to a real experiment:

$$\ln\frac{n_{i,t_c}}{n_{i,0}} = -\int\frac{\Phi_i}{\sqrt{T}}\exp\left(\frac{\Delta_f G}{-RT}\right)dt = -\sum_{u=1}^{N}\left[\frac{\Phi_i}{\sqrt{T_{u,u+1}}}\exp\left(\frac{\Delta_f G}{-RT_{u,u+1}}\right)(t_{u+1}-t_u)\right] \quad \text{(S11)}$$

where N is the number of temperature points recorded in the experiment, and $T_{u,u+1}$ is the average temperature of u*th* point and (u+1)*th* point recorded at the time t_u and t_{u+1}. By combining Eq. (S10) with Eq. (S11), the corrected duration could be calculated as:

$$t_c = \frac{\sum_{u=1}^{N}\left[\frac{(t_{u+1}-t_u)}{\sqrt{T_{u,u+1}}}\exp\left(\frac{\Delta_f G}{-RT_{u,u+1}}\right)\right]}{\exp\left(\frac{\Delta_f G}{-RT_0}\right)/\sqrt{T_0}} \quad \text{(S12).}$$

Since the sample mass loss was mainly due to the evaporation loss of SiO_2 (see the main text), we used the surface reaction: SiO_2 (melt) = SiO (gas) + $1/2O_2$ (gas) to correct the run duration. According to the data from the JANAF tables (Chase, 1998), the $\Delta_f G$ (in kJ/mol) for this reaction could be written as a function of T (Badro et al., 2021):

$$\Delta_f G_{SiO_2\text{-}SiO} = 759.72 - 0.232T \quad \text{(S13).}$$

Through the above methods, we corrected the effect of temperature fluctuation on the run duration at the target temperature. Large temperature fluctuation could lead to large difference between laser-on duration and corrected duration. For example, the run duration of run M08 was corrected from 420 s to 737 s because of the large temperature fluctuation (over ~400 K) at the beginning of the evaporation (Figure S1). This explains why sample M08 has a shorter heating time but a higher mass loss fraction compared to sample M09 (Table 1). Despite the large correction on run duration, run M08 still follows the same elemental and isotopic fractionation trends as the other samples, which implies that the temperature effect is limited (see main text for detailed discussion). It is also worth noting that the assumption that some parameters in Eq. (S8) are temperature-independent might not be exactly true for evaporation experiments. For example, a) the fO_2 is a function of temperature; b) the evaporation coefficients for silicate melts and their temperature-dependence are still poorly constrained; c) at temperatures >2000 K, the abundances of gaseous SiO_2 and O along with complex clusters might increase in the vapor (Shornikov & Yakovlev, 2015), and thus the M_i might also be temperature-dependent.

Text S2. Kinetics of silicate melt evaporation

Evaporation processes involve elements transferring inside the melt through diffusion and gaseous species escaping from the surface. The recovered samples were chemically homogenous (Figure 2), indicating that diffusion in the melt does not limit the evaporation process (Richter et al., 2002). We below highlight the kinetic process that the gaseous species escaped from the melt surface.

To levitate the sample during the experiments, the required velocity of the argon flow is given as (Badro et al., 2021):

$$U = \sqrt{\frac{8\rho_{melt}rg}{3C_x\rho_{gas}}} \quad \text{(S14)}$$

where g is Earth's gravity (9.8 m/s^2), C_x is the drag coefficient for a sphere (0.47), r is the sample radius, and ρ_{melt} and ρ_{gas} are the density of the melt and the argon gas, respectively. Given a melt density of 3200 kg/m^3, an argon gas density of 1.7 kg/m^3, and a typical sample radius of 1.5 mm in our experiments, the obtained U is ~13 m/s, which is the same as the argon flow rate estimated from our experimental setup independently (see Methods section). The argon flow around the levitated melt sphere could be characterized by Reynolds number $Re = UL/\nu$ (e.g., Badro et al., 2021), where L is the characteristic length of the flow (diameter of the sample in this study) and ν is the gas kinematic viscosity. The use of an argon ν of 10^{-4} m^2/s at 2523 K (Aissa et al., 2015) yielded a Re value of 390, indicating that the vapor flow around the levitated sample was laminar in our experiments.

The produced gaseous species during evaporation escape from the melt surface through

advection and diffusion. The relative magnitude of these two mechanisms (advection v.s. diffusion) could be described by the dimensionless Péclet number $Pe=UL/D_{i,j}$, where $D_{i,j}$ is the diffusion coefficient of evaporated species i with molar mass of m_i, in a gas j with mass of M_j, and could be expressed by using Chapman-Enskog theory derived from the Boltzmann equation as (Cussler, 2009):

$$D_{i,j} = \frac{3k_BT}{16P\pi\sigma_{ij}^2\Omega^{(1,1)}}\sqrt{2\pi N_A k_B T\left(\frac{1}{m_i}+\frac{1}{M_j}\right)} \quad \text{(S15)}$$

where k_B is the Boltzmann constant (1.38×10^{-23} J/K), N_A is Avogadro's Number (6.02×10^{23} mol^{-1}), T is the absolute temperature in K, P is the total pressure in bar, $\sigma_{i,j}$ is the average collision diameter distance of i and j (given by $(\sigma_i+\sigma_j)/2$), and $\Omega^{(1,1)}$ is a temperature-dependent collision integral. For gaseous SiO and Mg diffusing in argon gas at conditions of 1 bar and 2523 K, the $\Omega^{(1,1)}$ approximates 0.68 (Neufeld et al., 1972) and the $\sigma_{SiO,Ar}$ & $\sigma_{Mg,Ar}$ are 4.08 Å & 3.44 Å (Rappe et al., 1992), yielding $D_{SiO,Ar}$ and $D_{Mg,Ar}$ of ~18 cm^2/s and ~26 cm^2/s, respectively. The obtained Péclet numbers are in the range of 15−22 in our experiments. These values are much higher than those in previous experiments conducted in tube furnace (e.g., Pe = 0.1 in Sossi et al. (2019)) or vacuum furnace (Pe = 0), indicating that advection was the dominant mechanism for the release of gaseous species from the melt surface in our experiments.

Text S3. Derivation of Eq. (6) in the main text

For SiO_2 and MgO in the melt that evaporates to a gaseous SiO and Mg, respectively, the chemical reactions are (e.g., Badro et al., 2021; Wang et al., 2001):

$$SiO_2\ (melt) = SiO\ (gas) + 1/2\ O_2\ (gas)$$
$$MgO\ (melt) = Mg\ (gas) + 1/2\ O_2\ (gas)$$

the equilibrium constant of which are given as:

$$K_{Si} = \frac{P_{SiO,sat}(fO_2)^{1/2}}{X_{SiO_2}\gamma_{SiO_2}} \quad \text{(S16)}$$

$$K_{Mg} = \frac{P_{Mg,sat}(fO_2)^{1/2}}{X_{MgO}\gamma_{MgO}} \quad \text{(S17).}$$

By combining Eqs. (S16) and (S17) with Eq. (S6), the ratio of the evaporation flux between Si and Mg can be written as:

$$\frac{dn_{Si}}{n_{Si}} = \frac{\varepsilon_{SiO}\gamma_{SiO_2}(1-S_{Si})K_{Si}}{\varepsilon_{Mg}\gamma_{MgO}(1-S_{Mg})K_{Mg}}\sqrt{\frac{M_{Mg}}{M_{SiO}}}\frac{dn_{Mg}}{n_{Mg}} \quad \text{(S18).}$$

We can see from Eq. (S18) that the environmental factors, such as ρ_{melt}, T, and fO_2, were eliminated. Integrating Eq. (S18) on both sides with respect to dn_{Si} and dn_{Mg} yields:

$$ln\frac{n_{Si,t}}{n_{Si,0}} = \frac{\varepsilon_{SiO}\gamma_{SiO_2}(1-S_{Si})K_{Si}}{\varepsilon_{Mg}\gamma_{MgO}(1-S_{Mg})K_{Mg}}\sqrt{\frac{M_{Mg}}{M_{SiO}}}ln\frac{n_{Mg,t}}{n_{Mg,0}} \quad \text{(S19).}$$

On the left side of the Eq. (S19), $n_{Si,t}/n_{Si,0}$ is the residual fraction of Si at the time t, and could be written as $1-f_{Si}$, where f_{Si} is the loss fraction of Si. Doing the same for Mg on the right side and re-arranging Eq. (S19), the relationship between S_{Si} and S_{Mg} can be written as:

$$\frac{1-S_{Mg}}{1-S_{Si}} = \frac{\varepsilon_{SiO}\gamma_{SiO_2}K_{Si}\sqrt{M_{Mg}}}{\varepsilon_{Mg}\gamma_{MgO}K_{Mg}\sqrt{M_{SiO}}}\frac{\ln(1-f_{Mg})}{\ln(1-f_{Si})} \quad \text{(S20).}$$

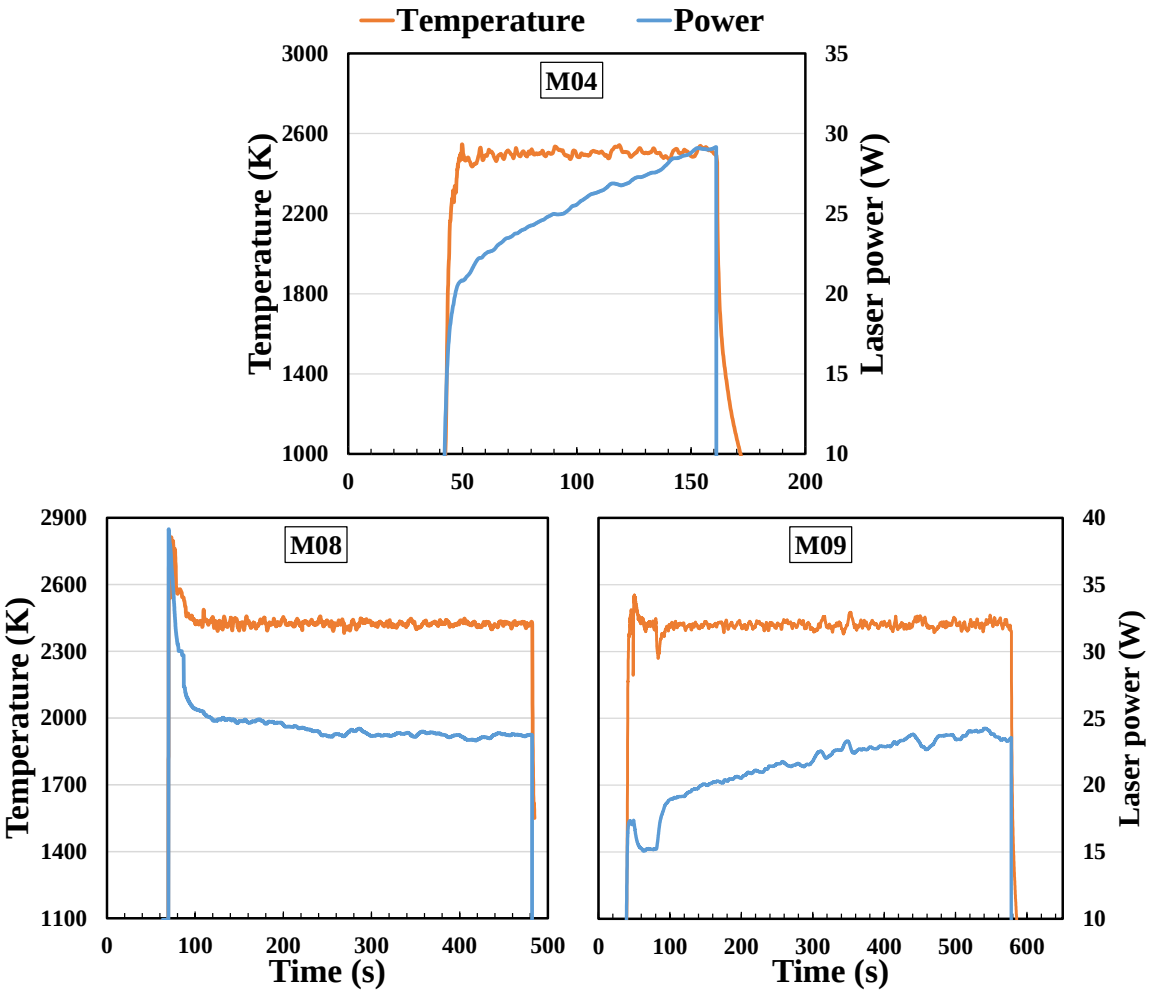

Figure S1. Diagrams showing the temperature (orange lines) and laser power (blue lines) change as the run duration in typical experiments. Note that sample M08 shows temperatures as high as 2800 K (~400 K higher than the target temperature) during heating in the first few seconds.

M01_2623K_2 mins:

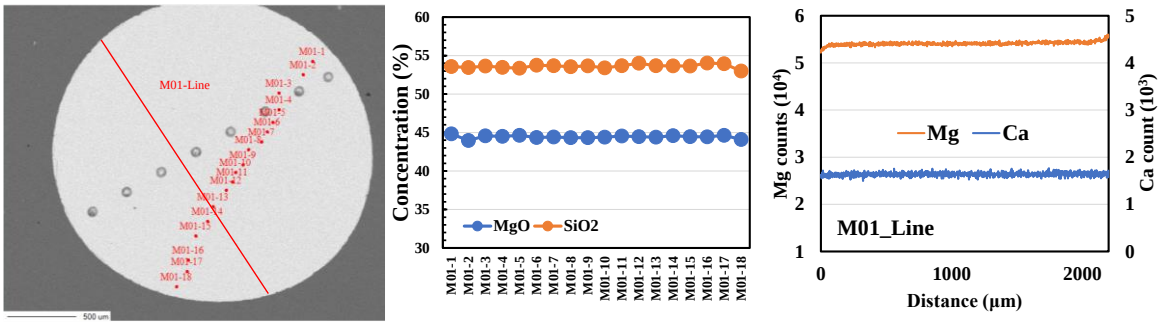

M05_2523K_5 mins:

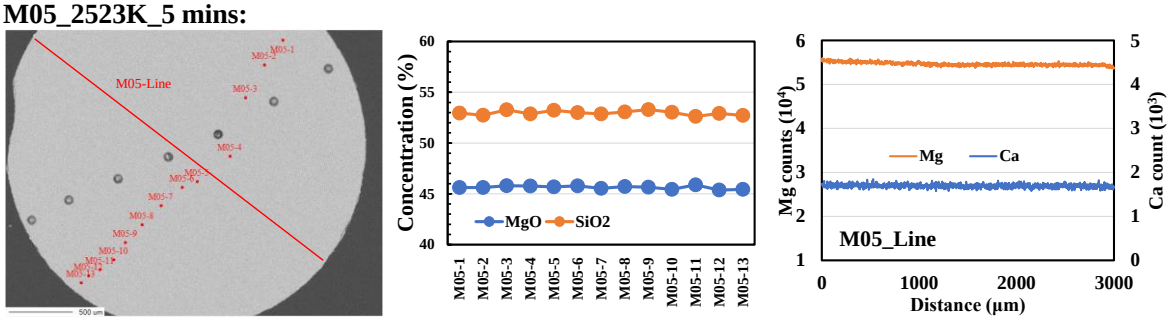

M07_2423K_5 mins:

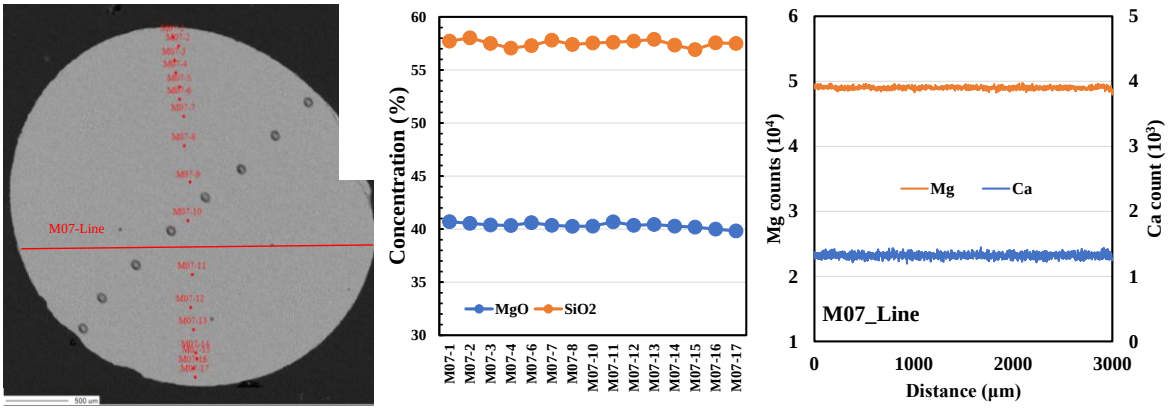

Figure S2. BSE images, point profiles, and line profiles of three typical recovery samples produced at different temperature and duration conditions. All the samples are homogeneous regardless of temperature and heating time. The black spots in the samples are the laser pits of LA–ICP–MS analysis.

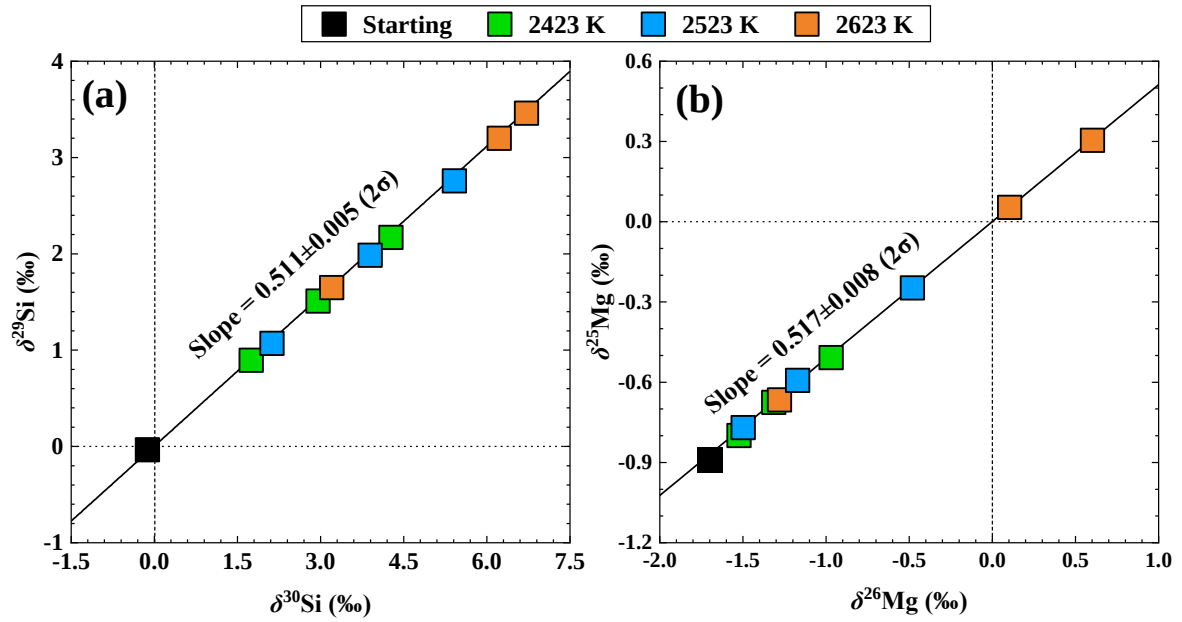

Figure S3. Diagrams showing no mass-independent isotopic fractionations of Si **(a)** and Mg **(b)** in our experiments. The uncertainties are within the symbols.

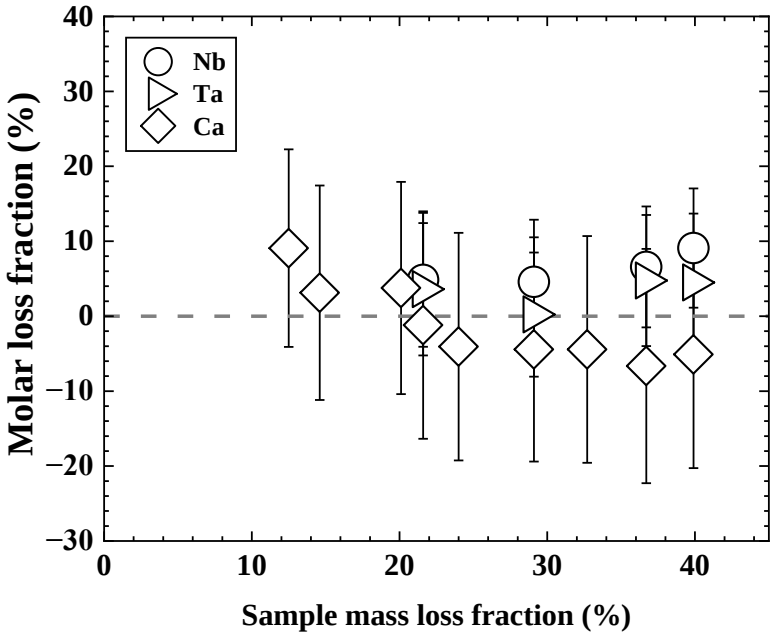

Figure S4. Calculated molar loss fraction of Ca, Nb, and Ta as a function of sample mass loss fraction. The uncertainties are 2σ.

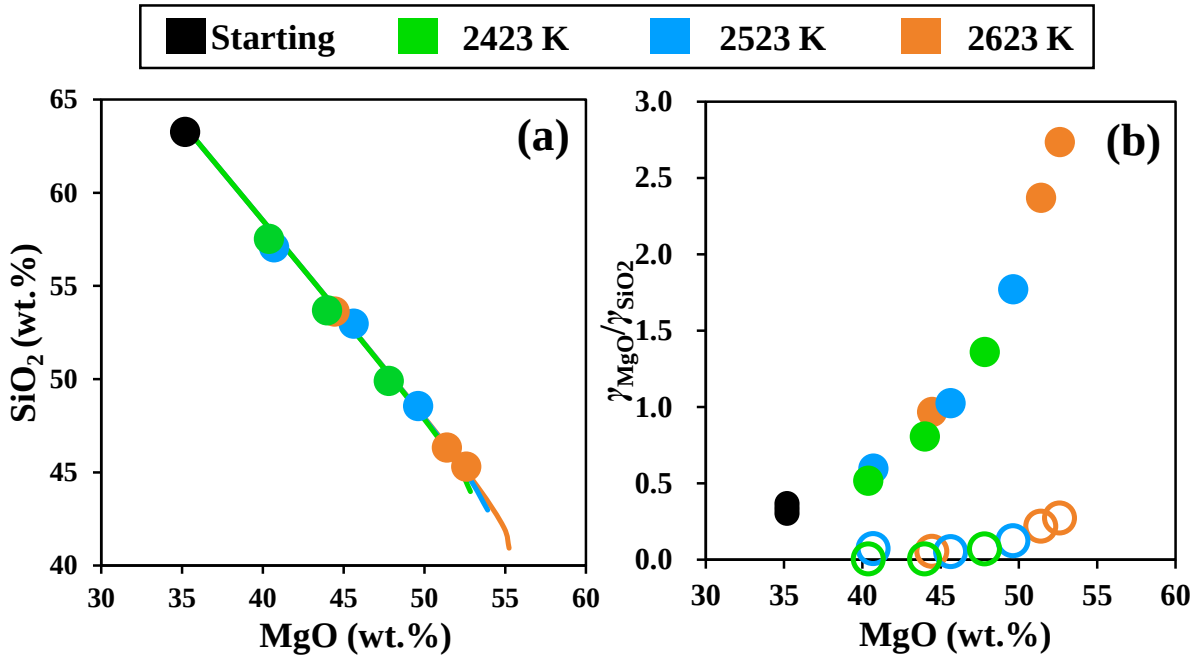

Figure S5. The SiO_2 content **(a)** and $\gamma_{MgO}/\gamma_{SiO2}$ **(b)** of the samples as a function of the MgO content. Plot **(a)** indicates that the variations of the SiO_2 and MgO contents in the recovered samples are consistent with the calculations (the curves) by using the MAGMA model (Fegley & Cameron, 1987; Schaefer & Fegley, 2004). Plot **(b)** shows the results of $\gamma_{MgO}/\gamma_{SiO2}$ calculated by using the MAGMA model (solid circles), which are compared with those calculated by using Eq. (6) and assuming $\varepsilon_{SiO}/\varepsilon_{MgO} \approx 1$ (open circles) as done by Badro et al. (2021). Note that the S_{Mg} at 2423 K, required for the calculation but not determined from our experiments, was assumed to be equal to that at 2523 K. The disparity may indicate that the assumption of $\varepsilon_{SiO}/\varepsilon_{MgO} \approx 1$ is not appropriate for enstatite melt evaporation. The observation that the $\gamma_{MgO}/\gamma_{SiO2}$ increases as the MgO content increases indicates a compositional effect on $\gamma_{MgO}/\gamma_{SiO2}$.

Table S1. Instrumental operating parameters for Si and Mg isotope measurements.

Instrument parameters	
RF power	1200 W
Cooling Ar	~ 16 L/min
Auxiliary Ar	~ 0.8 L/min
Nebulizer Ar	~ 1.0 L/min
Extraction voltage	-2000 V
Vacuum	4-8 × 10^{-9} Pa
Typical ^{24}Mg sensitivity	5-6 V/ppm (MR)
Background	< 1 mV
Cones	Ni (H), Jet sampler cone
Ion lens setting	Optimized for max. intensity
Sample uptake	~ 50 µl/min (^{28}Si, ^{24}Mg)

Table S2. Experimental isotopic fractionation factor (α_{exp}) and saturation degree (S) obtained from this study and previous studies.

Experimental method	**Starting material**	***T*(K)**	$\alpha_{exp}(^{29}Si/^{28}Si)$	**2σ**	$\alpha_{exp}(^{25}Mg/^{24}Mg)$	**2σ**	S_{Si}	**2σ**	S_{Mg}	**2σ**	$(Mg/Si)_{max}/(Mg/Si)_{ini}$	**Reference**
Laser-heated aerodynamic levitation furnace	Enstatite	2423-2623	0.99585	0.00002	0.98942	0.00130	0.662	0.002	0.459	0.068	2.16	This study
	Type B CAIs	1873	0.99700	0.00045	0.99500	0.00054	0.794	0.036	0.755	0.031	1.19	Badro et al. (2021)
Vacuum or near-vacuum furnace	Mg_2SiO_4	2323	0.99300	0.00039	0.98537	0.00083	0.412	0.035	0.249	0.043	1.00	Davis et al. (1990)
		2173	0.99245	0.00010	0.98417	0.00039	0.368	0.009	0.188	0.020	1.00	
	Solar nebular- like materials	2273	0.98994	0.00053	0.98325	0.00117	0.138	0.048	0.139	0.061	1.12	Wang et al. (2001)
		2073	0.99179	0.00051	0.98712	0.00299	0.313	0.046	0.343	0.156	1.05	
	Type B CAIs	2173	0.99040	0.00044	0.98607	0.00017	0.183	0.040	0.287	0.009	0.19	Richter et al. (2007) & Knight et al. (2009)
		2073	0.99040	0.00044	0.98709	0.00004	0.188	0.040	0.341	0.002	0.23	
		1873	0.99040	0.00044	0.98761	0.00014	0.200	0.040	0.371	0.007	0.04	
	Mg-rich FUN CAIs	2173	0.98990	0.00040	0.98372	0.00046	0.138	0.036	0.164	0.024	0.70	Mendybaev et al. (2013)
	Si-rich FUN CAIs	2173	0.98990	0.00040	0.98567	0.00041	0.138	0.036	0.266	0.021	0.11	
	FUN CAIs	2173	0.99010	0.00038	0.98383	0.00033	0.156	0.034	0.170	0.017	0.56	Mendybaev et al. (2017)
	CAI-like silicates	1873	0.99100	0.00050	0.98770	0.00040	0.254	0.045	0.376	0.021	0.33	Mendybaev et al. (2021)

References of supplementary materials

Aissa, A., Abdelouahab, M., Noureddine, A., Elganaoui, M., & Pateyron, B. (2015). Ranz and Marshall correlations limits on heat flow between a sphere and its surrounding gas at high temperature. *Thermal Science*, *19*(5), 1521–1528.

Badro, J., Sossi, P. A., Deng, Z., Borensztajn, S., Wehr, N., & Ryerson, F. J. (2021). Experimental investigation of elemental and isotopic evaporation processes by laser heating in an aerodynamic levitation furnace. *Comptes Rendus. Géoscience*, *353*(1), 101–114. https://doi.org/10.5802/crgeos.56

Cussler, E. L. (2009). *Diffusion: Mass Transfer in Fluid Systems*. Cambridge University Press.

Dauphas, N., Poitrasson, F., Burkhardt, C., Kobayashi, H., & Kurosawa, K. (2015). Planetary and meteoritic Mg/Si and δ 30 Si variations inherited from solar nebula chemistry. *Earth and Planetary Science Letters*, *427*, 236–248. https://doi.org/10.1016/j.epsl.2015.07.008

Fegley, B., & Cameron, A. G. W. (1987). A vaporization model for iron/silicate fractionation in the Mercury protoplanet. *Earth and Planetary Science Letters*, *82*(3–4), 207–222. https://doi.org/10.1016/0012-821X(87)90196-8

Neufeld, P. D., Janzen, A. R., & Aziz, R. A. (1972). Empirical Equations to Calculate 16 of the Transport Collision Integrals Ω(l, s)* for the Lennard-Jones (12–6) Potential. *The Journal of Chemical Physics*, *57*(3), 1100–1102. https://doi.org/10.1063/1.1678363

Ni, P., Macris, C. A., Darling, E. A., & Shahar, A. (2021). Evaporation-induced copper isotope fractionation: Insights from laser levitation experiments. *Geochimica et Cosmochimica Acta*, *298*, 131–148. https://doi.org/10.1016/j.gca.2021.02.007

Rappe, A. K., Casewit, C. J., Colwell, K. S., Goddard, W. A., & Skiff, W. M. (1992). UFF, a full periodic table force field for molecular mechanics and molecular dynamics simulations. *Journal of the American Chemical Society*, *114*(25), 10024–10035. https://doi.org/10.1021/ja00051a040

Richter, F. M., Davis, A. M., Ebel, D. S., & Hashimoto, A. (2002). Elemental and isotopic fractionation of Type B calcium-, aluminum-rich inclusions: experiments, theoretical considerations, and constraints on their thermal evolution. *Geochimica et Cosmochimica Acta*, *66*(3), 521–540. https://doi.org/10.1016/S0016-7037(01)00782-7

Richter, F. M., Janney, P. E., Mendybaev, R. A., Davis, A. M., & Wadhwa, M. (2007). Elemental and isotopic fractionation of Type B CAI-like liquids by evaporation. *Geochimica et Cosmochimica Acta*, *71*(22), 5544–5564. https://doi.org/10.1016/j.gca.2007.09.005

Schaefer, L., & Fegley, B. (2004). A thermodynamic model of high temperature lava vaporization on Io. *Icarus*, *169*(1), 216–241. https://doi.org/10.1016/j.icarus.2003.08.023

Shornikov, S. I., & Yakovlev, O. I. (2015). Study of complex molecular species in the gas phase over the CaO–MgO–Al2O3–TiO2–SiO2 system. *Geochemistry International*, *53*(8), 690–699. https://doi.org/10.1134/S0016702915080066

Sossi, P. A., Klemme, S., O'Neill, H. St. C., Berndt, J., & Moynier, F. (2019). Evaporation of moderately volatile elements from silicate melts: experiments and theory. *Geochimica et Cosmochimica Acta*, *260*, 204–231. https://doi.org/10.1016/j.gca.2019.06.021

Wang, J., Davis, A. M., Clayton, R. N., Mayeda, T. K., & Hashimoto, A. (2001). Chemical and isotopic fractionation during the evaporation of the FeO-MgO-SiO2-CaO-Al2O3-TiO2 rare earth element melt system. *Geochimica et Cosmochimica Acta*, *65*(3), 479–494. https://doi.org/10.1016/S0016-7037(00)00529-9